



Additive Manufacturing of Biologically-inspired Materials

Journal:	<i>Chemical Society Reviews</i>
Manuscript ID	CS-REV-11-2015-000836.R1
Article Type:	Review Article
Date Submitted by the Author:	03-Jan-2016
Complete List of Authors:	Studart, Andre; ETH Zurich,

Additive Manufacturing of Biologically-Inspired Materials

André R. Studart

Complex Materials, Department of Materials, ETH Zürich, 8093 Zürich, Switzerland

Abstract

Additive manufacturing (AM) technologies offer an attractive pathway towards the fabrication of functional materials featuring complex heterogeneous architectures inspired by biological systems. In this paper, recent research on the use of AM approaches to program the local chemical composition, structure and properties of biologically-inspired materials is reviewed. A variety of structural motifs found in biological composites have been successfully emulated in synthetic systems using inkjet-based, direct-writing, stereolithography and slip casting technologies. The replication in synthetic systems of design principles underlying such structural motifs has enabled the fabrication of lightweight cellular materials, strong and tough composites, soft robots and autonomously shaping structures with unprecedented properties and functionalities. Pushing the current limits of AM technologies in future research should bring us closer to the manufacturing capabilities of living organisms, opening the way for the digital fabrication of advanced materials with superior performance, lower environmental impact and new functionalities.

Introduction

Additive manufacturing (AM) technologies offer a versatile platform for the on-demand fabrication of customized products in a decentralized and cost-effective fashion.¹ Besides its traditional use as a tool for rapid prototyping or for the small-scale production of customized items, additive manufacturing has also been exploited as a means to fabricate components with unusual shapes in a wide range of fields from architecture to medicine to anthropology.²⁻⁶

An even more enticing feature that has only recently started to be explored is the use of AM technologies to create materials with locally tuned chemical compositions and intricate microstructures that are not accessible by conventional processing routes.⁷⁻¹⁴ The exploration of this feature has been driven and inspired by the complex architectures of biological materials made by living organisms in nature. Because they have been highly optimized through hundreds of millions of years of natural evolution to meet specific functional demands, such natural architectures exhibit structural features that find no counterparts among man-made materials.

Examples of such structural features are the anisotropic building blocks with optimized size and aspect ratio, the hierarchical organization of building blocks over multiple length scales, the combination of strong and weak bonds between building blocks to enable dynamic functionalities (adaptation, remodeling, self-healing), and the controlled spatial distribution and orientation of building blocks into heterogeneous and graded architectures.¹⁵⁻²² Optimization of these features through natural evolution to fulfill specific functional demands of the environment has led to the rich library of structural motifs that can be found in biological materials.

Some examples of structural motifs exhibiting different orientation of reinforcing building blocks in dense and porous biological materials across different kingdoms and phyla are shown in Figure 1. This represents just a small exemplary sample of motifs covering only one of the structural features described above. Utilizing AM tools to mimic some of these structural features in exquisite heterogeneous architectures may open the way towards the fabrication of bioinspired materials that outperform today's synthetic counterparts or that meet the desired function using more environmental-benign or biologically-compatible resources.¹⁵ Moreover, bioinspired materials made by AM can be used as model systems to investigate the design principles that has guided the evolution of the biological nano-/microstructures into the different structural motifs found in natural materials.

The potential of AM technologies in replicating structural features of biological materials in synthetic components lies in their intrinsic ability to spatially control the local microstructure and chemical composition from the bottom up in a layer-by-layer fashion. Interestingly, such a layer-by-layer synthetic approach share common features with the way living organisms sequentially deposit matter to build biological materials in nature (Figure 2). These common features include: (1) the supply of building blocks in a continuous or stepwise manner, (2) a programming code that determines the macroscopic shape and local heterogeneity of the material to be assembled, (3) mechanisms to implement the code and thus control the chemistry and orientation of deposited building blocks, and (4) a consolidation step that fixes the deposited material in place in the form of heterogeneous layered or pixelated architectures.

Although man-made technologies are still far from reaching the level of intricacy and precision present in biological systems, the common features highlighted above suggest that additive manufacturing offer an exciting route towards the creation of synthetic heterogeneous materials with increasing levels of complexity and functionalities. The plethora of synthetic heterogeneous structures that can be potentially generated is illustrated by the rich diversity of tissues and materials found in nature.

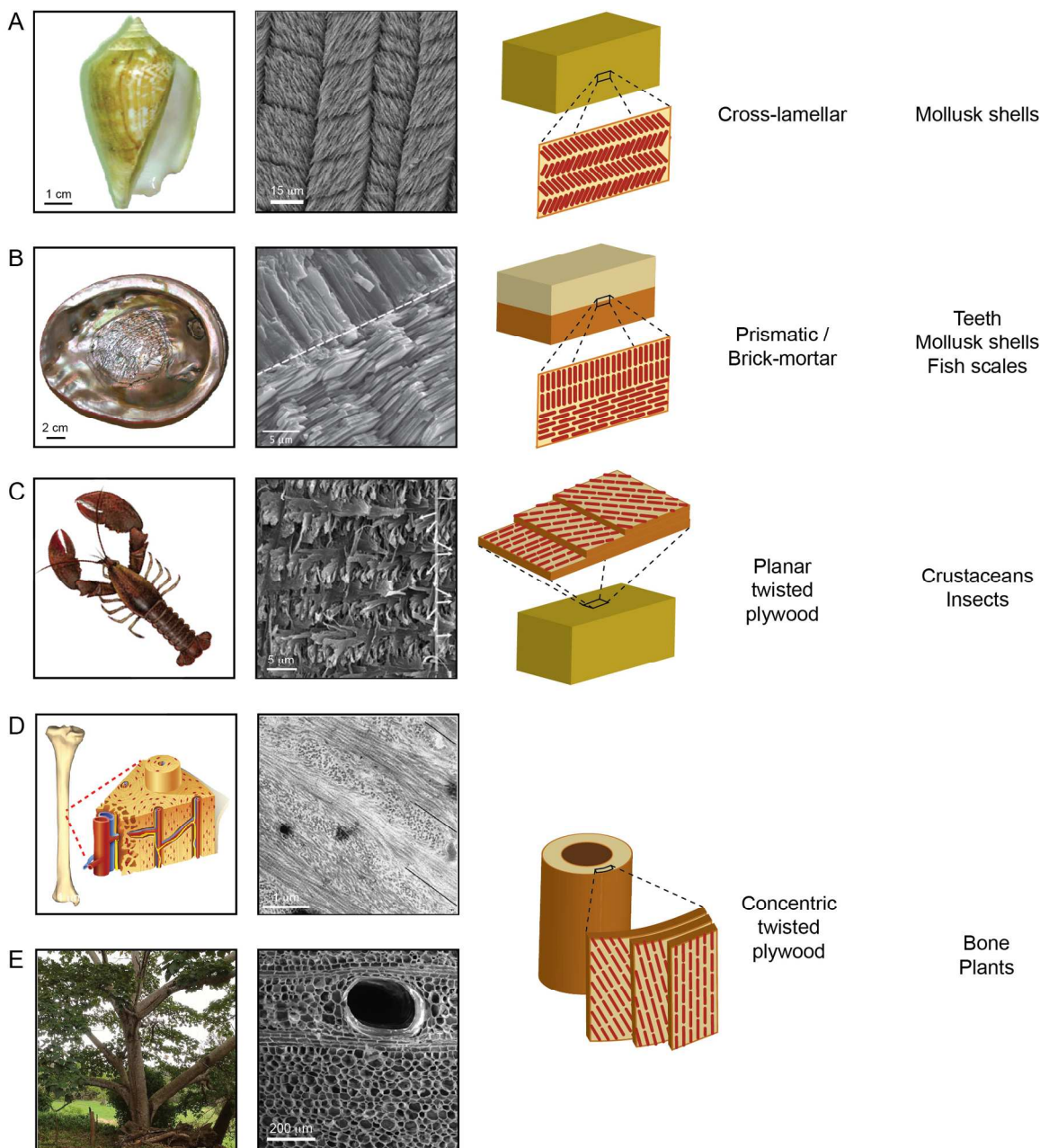


Figure 1. Examples of universal structural motifs found in biological materials. A. Cross-lamellar architecture found in mollusk shells. Adapted with permission from Pokroy *et al.*²³ B. Combined prismatic and brick-and-mortar structures encountered in teeth, mollusk shells and fish scales. Mollusk picture adapted with permission from Barthelat *et al.*²⁴ SEM image adapted with permission from Kröger.²⁵ C. Planar twisted plywood pattern grown within the partially-mineralized and non-mineralized exoskeletons of crustaceans and insects, respectively. Photograph (left) shows the lobster *Homarus americanus*.²⁶ SEM image (right) was adapted with permission from Fabritius *et al.*²⁷ D,E. Concentric twisted plywood architecture found around vessels permeating the structure of bone and plants. D depicts schematically an osteon inside

cortical bone (left) and a bone cross-section displaying the characteristic twisted plywood projected pattern (right). The bone drawing (left) is distributed under the Creative Commons Attribution-Share Alike 2.1 Japan license.²⁸ The TEM image (right) was adapted with permission from Weiner *et al.*²⁹ E shows a picture of the balsa tree *Ochroma pyramidale* (left) and the cellular architecture of balsa wood (right). The tree photograph (left) was taken by Gabriele Kothe-Heinrich and is distributed under a Creative Commons Attribution-Share Alike 3.0 Unported license.³⁰ The SEM image (right) was adapted with permission from Borrega *et al.*³¹

In this paper, recent studies on the fabrication of bio-inspired materials through additive manufacturing technologies are reviewed to illustrate the potential of this approach in creating bioinspired heterogeneous materials with unprecedented architectural control. Several different AM technologies are covered, including established ink-jet and stereolithography platforms, versatile direct ink writing techniques and a recently proposed layer-by-layer casting approach. Despite the exciting developments in the field of bioprinting of living tissues, the review is focused on AM processes that utilize inks that do not contain living cells. Such processes benefit from the greater freedom in materials selection and processing conditions that is often lacking in bioprinting technologies. This flexibility allows for the fabrication of bioinspired materials for a wider range of applications and should also help identify materials and processing routes that would also be applicable to bio-printing.

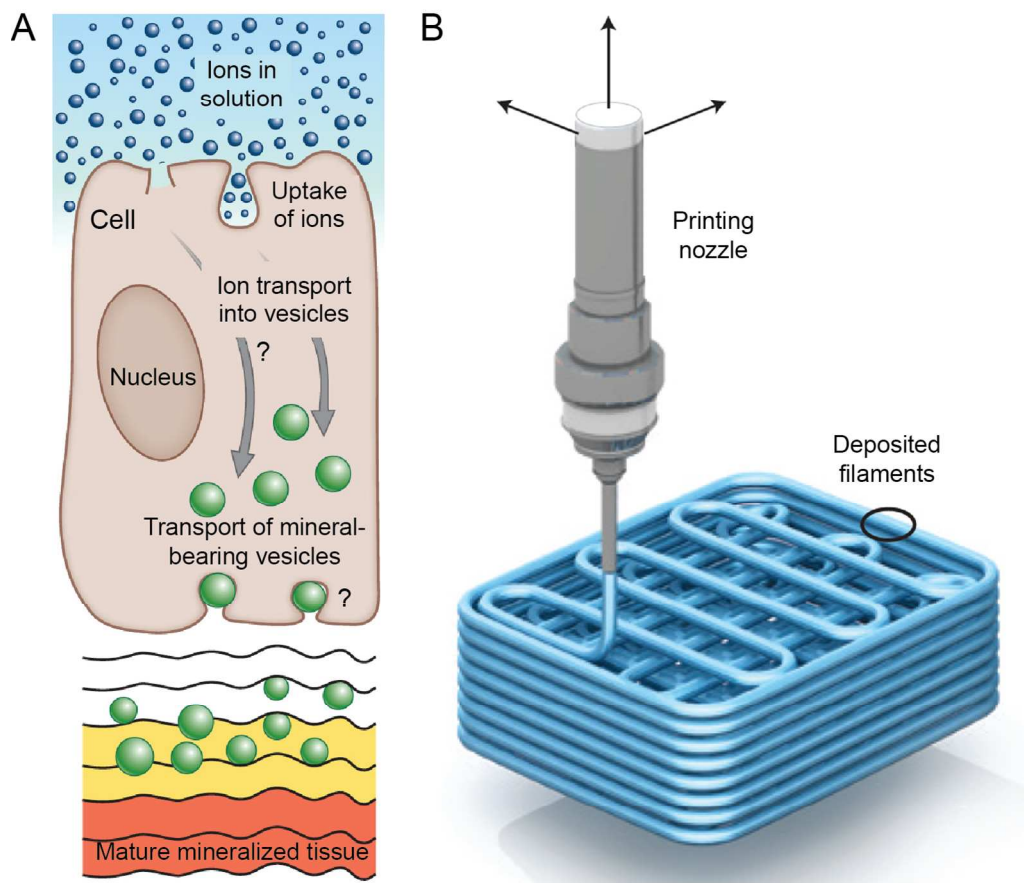


Figure 2. Comparison between biomineralization of a biological tissue (left) and 3D printing of a synthetic cellular material (right), revealing the analogous layer-by-layer additive approach in two otherwise very distinct manufacturing processes. In biomineralization, discrete packages of inorganic material are secreted by the cell to create the mineral phase within a pre-structured organic scaffold. In 3D printing, material is deposited in the form of a continuous filament (shown above) or as discrete droplets to build structures layer by layer. Adapted with permission from Weiner *et al.*³² and Wegst *et al.*³³

PolyJet 3D printing

PolyJet 3D printing is a well-established ink jet technology that offers the possibility of multi-material deposition using commercially-available equipment.^{10, 34-37} The method consists in dispensing droplets of liquid monomers or oligomers that are polymerized upon UV illumination right after deposition onto a build tray (Figure 3A). In addition to the material of interest, a support material is used during the printing process to allow for the formation of overhangs and is subsequently removed through simple washing. Compared to the continuous filaments produced

by extrusion-based techniques (discussed below), ink jet printing offers a lot of opportunities in terms of local compositional control. This stems from the fact that the local composition can be deliberately chosen by adjusting the relative fraction of printed droplets. Such flexibility enables the fabrication of heterogeneous materials comprising individual voxels with well-defined composition and properties.

The outstanding capabilities of multi-material ink jet printing has been recently exploited to fabricate stiff and flexible protective armors inspired by the exoskeleton of ancient fish,³⁶ self-shaping cellular structures analogous to morphing natural seedpods,³⁵ a combustion-powered soft robot with functionally graded body,³⁷ flexible biomimetic shark skin with tailor-made surface roughness^{38,39} and a range of structural components that replicate the design features of bone and biogenic calcite^{10,34} (Figure 3B-F). The printed objects in these examples are typically made at the centimeter scale, with minimum feature sizes approaching a few tens of micrometers.¹⁰

Here, multi-material bioinspired architectures are compared to illustrate the potential of this additive manufacturing route in generating polymer-based synthetic composites that combine antagonistic properties, such as strength and fracture toughness. These mechanical properties are often mutually exclusive and thus difficult to reach in homogeneous materials.⁴⁰ Instead, multi-material ink jet printing enables the fabrication of simultaneously strong and tough structural components using monomer inks that would lead to weak and soft or brittle and stiff polymers if made homogeneous. Heterogeneous composites that combine stiff reinforcing elements with a soft organic matrix have been successfully exploited for decades in the form of glass or carbon fiber reinforced polymers.^{41,42} Compared to this established technology, multi-material printing offers the possibility of cost-effective automation of the fabrication process and provides greater flexibility to locally design the composite architecture in three dimensions. Design flexibility in terms of site-specific composition and texture can be exploited to generate new functionalities and interactivity with the environment (e.g. morphing, self-healing, adaptation)^{13,43} and to best respond to non-uniform mechanical loads developed during use.¹⁴

Among the different model bioinspired architectures that have been printed (Figure 3), we focus on the brick-and-mortar architecture found in bone and mollusk shells.^{10,34} Combined experiments and computer simulations on the fracture behavior of an ink-jet printed bone-like plate (Figure 4) reveals that toughness in this bio-inspired architecture emerges from the synergetic effects of a load-bearing stiff anisotropic phase (bricks) and a soft and ductile polymer matrix (mortar). Computation of local deformations within the material during mechanical loading of notched plates indicates that the soft polymer phase present along the short length of the anisotropic stiff elements is extensively strained during the fracture process (Figure 4B,C). Interestingly, such local deformation is not limited to the volume of material around the notch, but is also observed at the top of the specimen further away from the area expected to concentrate the externally applied stress. This confirms the key role of the soft matrix in distributing the global

stresses throughout a large volume of the loaded material, delocalizing the fracture initiation process. Fracture is also delayed by significant blunting of the crack tip, resulting from the high ductility of the soft polymer. Eventually, the fracture strain of the highly deformed soft phase is locally reached, resulting in several fracture sites across the entire specimen. Such multiple fracture sites are observed both in experiments and simulations (Figure 4A,B).

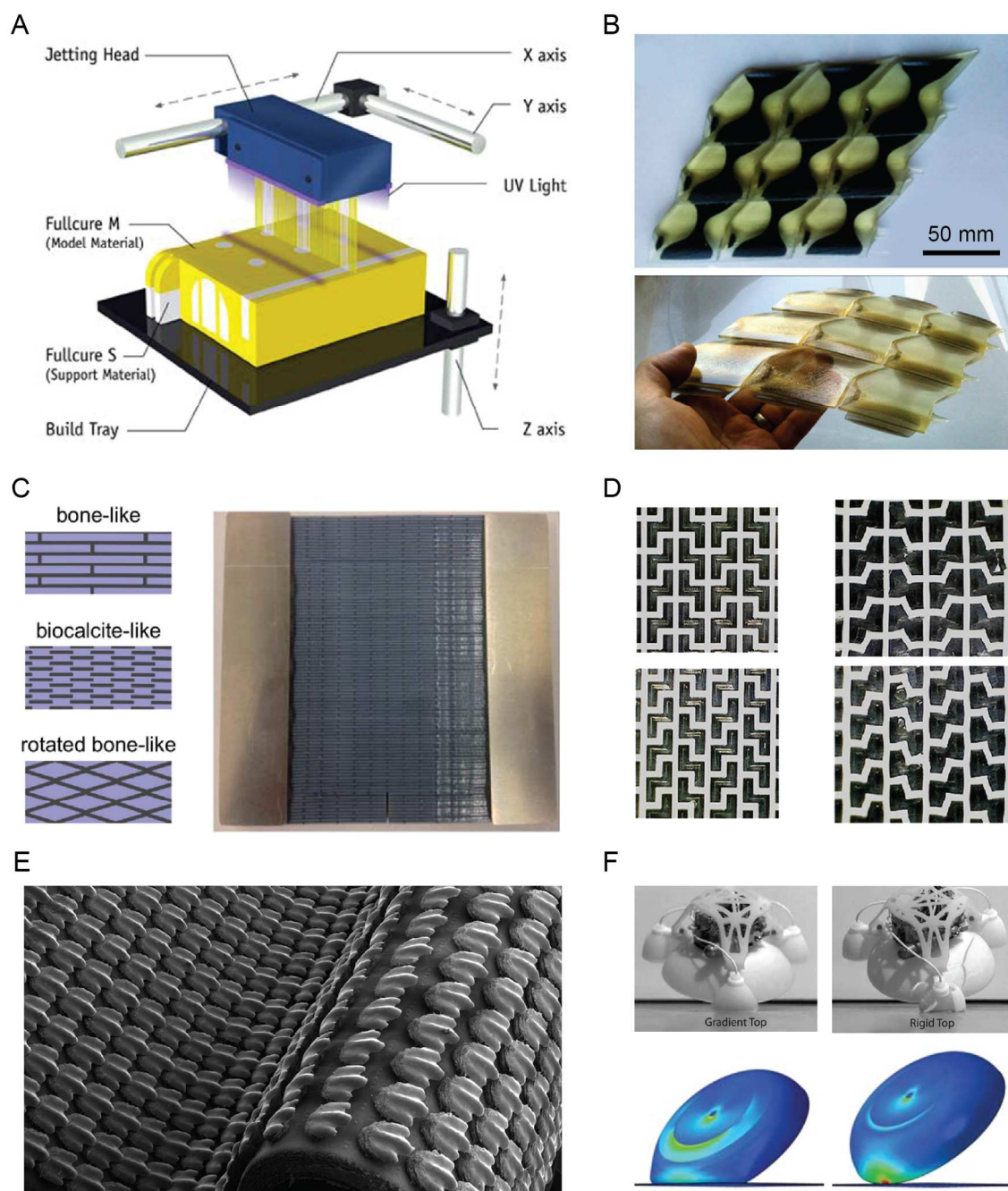


Figure 3. PolyJet 3D printing technology and bioinspired composites obtained using its multi-material capabilities. A. Schematics of the hardware used in the PolyJet technology (courtesy of

Dr. Daniel Dikovsky, Stratasys). B. Printed composite inspired by the articulated armored scale-jacket system of an ancient fish. Adapted with permission from Araya *et al.*³⁶ C. Bioinspired structural motifs printed using a combination of soft and hard polymers (left) and a photograph of an exemplary bone-like 3D printed composite (right, typical width \approx 6 cm). Adapted with permission from Dimas *et al.*^{10, 34} D. Periodic honeycomb structures inspired by the actuation mechanism of plants, shown before (left) and after (right) swelling in a solvent. Adapted with permission from Guiducci *et al.*³⁵ E. 3D printed membrane comprising rigid denticles on a flexible substrate to mimic the skin of sharks. Each denticle measures approximately 1.5 mm. Adapted with permission from Wen *et al.*³⁸ F. Combustion-propelled soft robots exhibiting intact, graded or broken, rigid top structures (left and right, respectively). Simulations (bottom) show that the mechanical gradient reduces stress concentration in the structure during landing impact. Simulated von Mises stresses range from zero (blue) to 20 MPa (red). Adapted with permission from Bartlett *et al.*³⁷

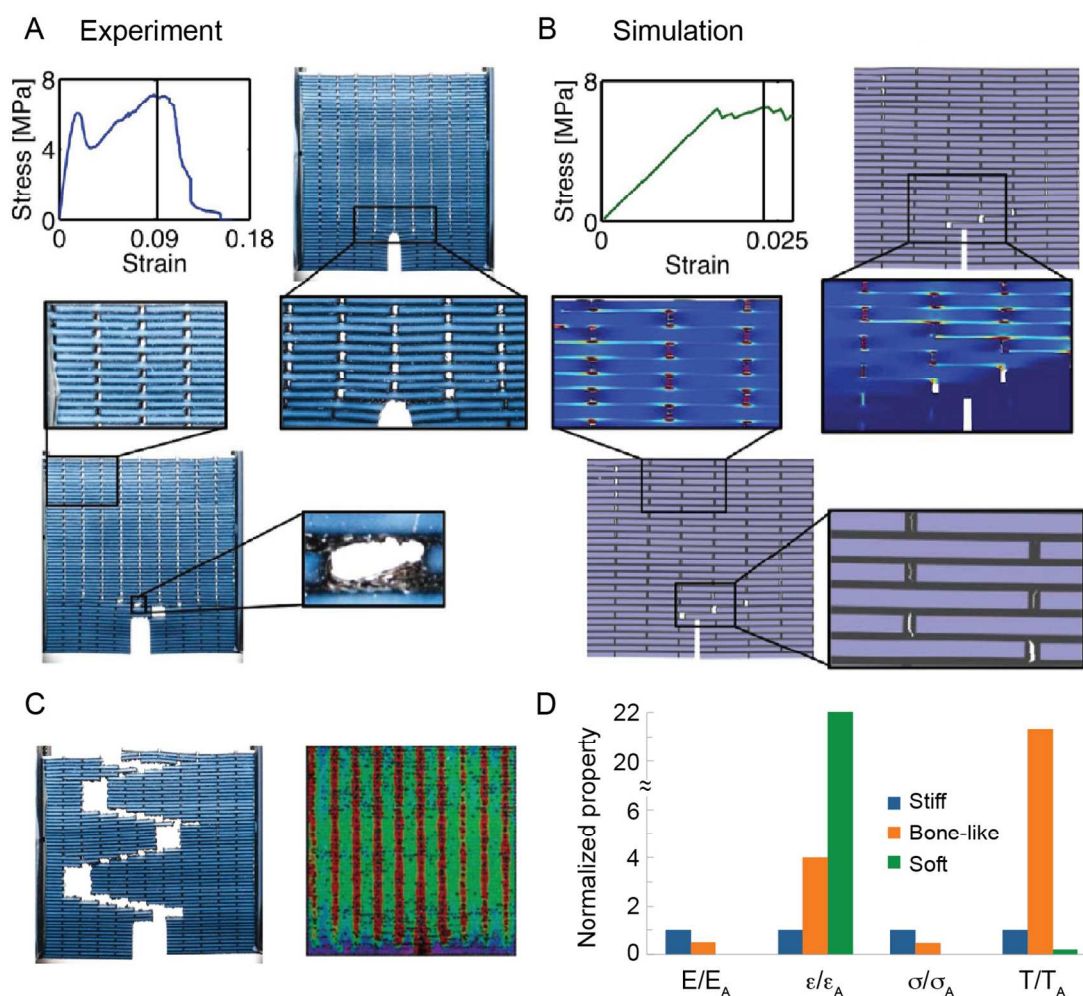


Figure 4. Experimental and simulated fracture behavior of 3D printed bone-like composites exhibiting a brick-and-mortar architecture.^{10, 34} A,B. Stress-strain responses and snapshots illustrating the deformation mechanisms observed in (A) experiments and (B) simulations. C. Tortuous path of a crack that propagated through the brick-and-mortar structure (left) and digital image correlation (DIC, right) depicting the highly deformed sites localized between bricks (in red). D. Experimentally determined mechanical properties of the bone-like composite as compared to those of the soft and stiff constituent materials alone. E is the stiffness, ε is the maximum strain, σ is the maximum stress, and T is the modulus of toughness (area under the stress-strain curve). Data were normalized with respect to the properties of the stiff constituent (index A). Adapted with permission from Dimas *et al.*^{10, 34}

Because of its stiff nature, the staggered bricks take up part of the mechanical load applied to the polymer matrix through stress transfer by shear at the brick-mortar interface.⁴⁴⁻⁴⁶ This increases the global resistance of the material against deformation, enhancing the overall stiffness and strength of the composite. Most importantly, the presence of stiff bricks arranged in a staggered fashion forces fracture of the material along the softer polymer phase. This leads to extensive deflection events at the brick-mortar interface that significantly increases the tortuosity of the crack path and thus the toughness of the composite (Figure 4C).^{10, 34}

The phenomena of strain delocalization, crack deflection and stress transfer at the brick-mortar interface makes the bone-like composites much tougher than their constituent materials alone (Figure 4D). As opposed to the elastic modulus and the fracture strength, the simulated and experimentally-determined toughness of the bio-inspired architectures is at least an order of magnitude higher than the level expected from a simple rule of mixture calculation.¹⁰ These results arise from synergetic effects similar to those responsible for the high fracture toughness of natural bone and well illustrates the potential of additive manufacturing in replicating in synthetic composites key design concepts present in strong and tough biological materials. Further improvements in the mechanical behavior of the brick-mortar architecture are expected upon reduction of the size of the stiff elements and the incorporation of asperities,⁴⁷ waviness^{24, 48} and rigid bridges connecting the load-bearing bricks.⁴⁹ The incorporation of such physical interlocking features and the potential to modify the surface chemistry of building blocks during the deposition process makes additive manufacturing technologies powerful tools to also control the interfacial properties of bioinspired composites.

Besides the biomimetic examples described here, the possibility to combine multiple materials in discrete droplets makes PolyJet printing a very attractive platform for the fabrication of many other heterogeneous composites. To exploit this feature and further advance the technology, new digital workflows have been developed to enable the assignment of site-specific materials properties to individual voxels within a 3D heterogeneous object.^{50, 51}

Although the unique voxel-based deposition concept of multi-material ink-jet technologies offers a lot of room for further exploration, such additive manufacturing approach is currently not the most suited for the deposition of inks loaded with high volume fractions of particles. This is related to the costly and delicate nature of the dispensing system, which makes particle clogging a major issue.⁵² Moreover, the fact that the printing hardware and currently available inks are proprietary and expensive imposes some restrictions in the development and open exploration of new formulations.⁵³ Given that anisotropic particles are a key structural element in most biological composites, additive manufacturing technologies that are more friendly towards particle-loaded formulations and allow for open-source development are a compelling complementary alternative to the established ink jet technology.

Direct ink writing (DIW)

Direct ink writing has been successfully utilized for the additive manufacturing of objects with a wide range of geometries, sizes and materials.⁵⁴⁻⁵⁸ Similarly to the fused deposition modeling approach used in popularized, low-cost printers, direct ink writing is an extrusion-based technique that delivers material through a syringe nozzle in the form of a continuous viscoelastic filament, which is consolidated via a chemical or physical mechanism after deposition in a printing tray (Figure 5A). Direct ink writing has been broadly disseminated due to its flexibility in terms of hardware and software combined with the availability of low-cost materials and nozzles. Inexpensive hardware and open-source software developed for fused deposition modeling can be readily utilized for direct ink writing, whereas the cheap and disposable nozzles used for materials dispensing makes particle clogging a more tolerable issue.

The key requirement for successful direct ink writing lies in the formulation of inks with optimum rheological behavior.⁵⁹ The ink has to be sufficiently fluid to allow for easy flow under the shear stresses applied during the extrusion process and at the same time exhibit enough elasticity to prevent flow and deformation of the deposited material when shearing ceases. Such rheological response is often achieved through chemical reactions, phase transitions and/or particle agglomeration within the ink prior to or shortly after the deposition process.⁵⁹⁻⁶³ Different approaches have been reported to fulfil this rheological requirement. For example, inks can be formulated to gel when extruded into a coagulation reservoir with specific liquid composition.^{60, 61} Such formulations are typically Newtonian and show shear viscosities in the order of 10^0 to 10^2 Pa.s, depending on the desired feature sizes. Other inks are deliberately designed to exhibit non-Newtonian viscoelastic response, thus enabling the fabrication of spanning structures, undistorted filaments and overhangs without *in situ* coagulation. Printing of spanning filaments requires inks with sufficiently high storage modulus to prevent excessive deflection under the action of gravity.

^{59, 62, 63} Although the minimum storage modulus depends on filament diameter, ink density and span distance, reported values are typically higher than a few kPa. Besides the effect of gravity, capillary forces can also lead to distortion of single filaments or multi-layered overhang structures. For an exemplary particle-loaded ink with surface tension of approximately 0.02 N/m, recent work has shown that a counteracting yield stress in the order of 100 Pa is needed to prevent shape distortion of single filaments and overhangs with radii of curvature of 200 μm .¹³

The capability of direct ink writing to easily print particle-loaded materials was recently utilized to manufacture cellular structures that replicate some of the architectural features of balsa, as an example of a lightweight natural composite (Figures 5 and 6).⁹ Two key structural features were mimicked: the low-weight cellular architecture of the overall object and the reinforcement of the walls of the cellular structure with stiff fibers. The low weight of balsa stems from the arrangement of the plant cells in a honeycomb-type porous structure (Figure 1E).⁶⁴ Because the printing ink can be made sufficiently elastic to enable building of undistorted filaments, DIW is particularly suited for the fabrication of cellular architectures that resemble the structure of balsa wood. Examples of polymer-based cellular structures with different cell designs printed by DIW are displayed in Figure 5C. The low-shear elasticity and yield stress that allows for printing of such structures was achieved in this exemplary case by incorporating nano-clay platelets into the pure epoxy resin used as polymer matrix (Figure 5D). The addition of clay changes the rheology of the resin from Newtonian to viscoelastic. In Figure 5D, the clay-containing resin is referred to as the base epoxy ink. The viscoelastic response of such base ink is evidenced by its high storage modulus (G') relative to the loss modulus (G'') at low shear stresses and the inversion of the moduli (fluidization) when the material is sheared beyond the critical point characterized by the yield stress (Figure 5D).

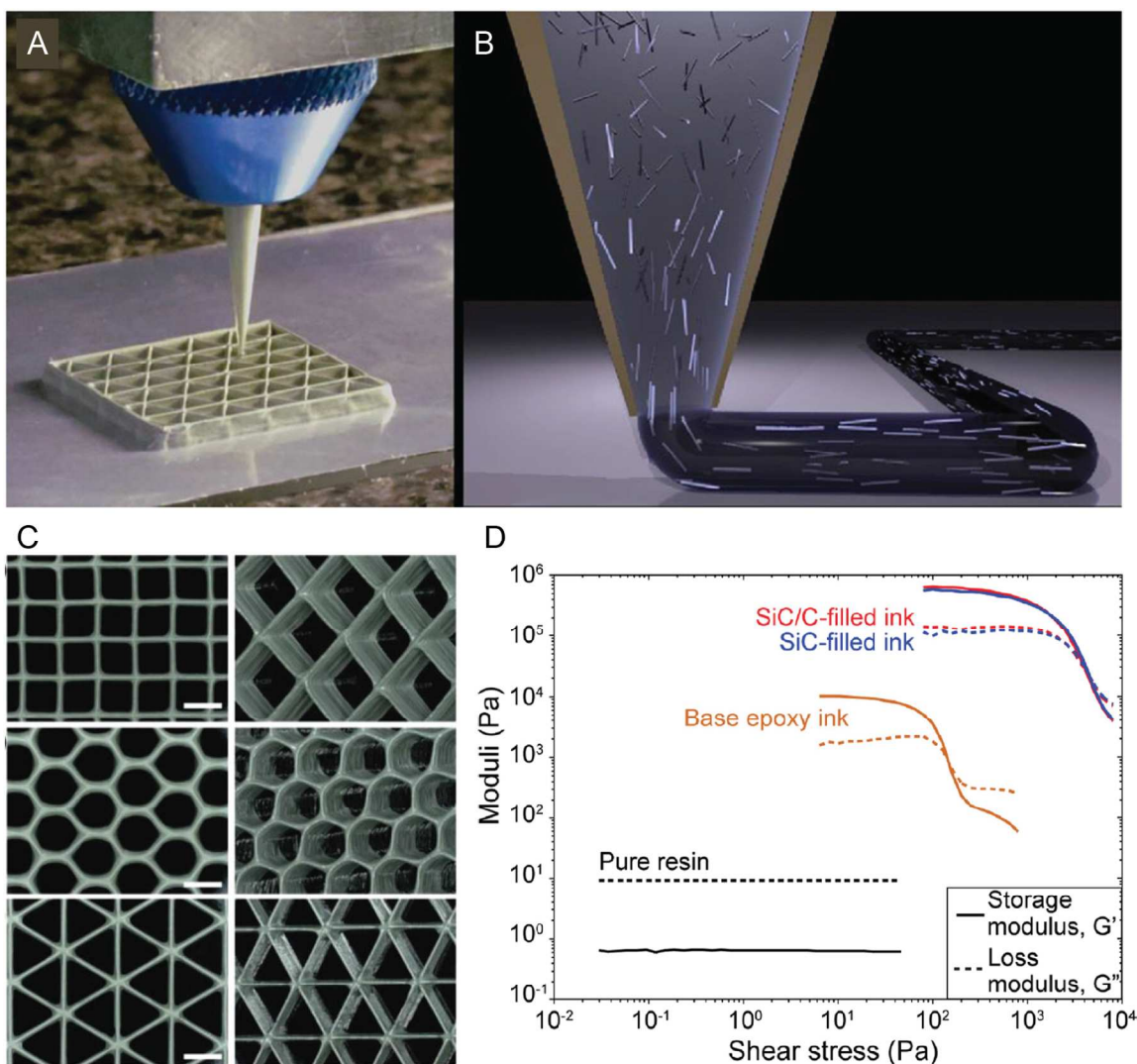


Figure 5. Direct ink writing (DIW) of cellular composites reinforced with stiff fibers and whiskers.⁹ A. Optical image showing the 3D printing of a triangular cellular structure. B. Schematics depicting the alignment of anisotropic particles due to shear at the dispensing nozzle. C. Examples of SiC-reinforced epoxy composites with cellular architectures of different geometries. Scale bars, 2mm. D. Rheological behavior of the epoxy-based inks used to print the cellular structures shown in C. The base epoxy ink is obtained by incorporating clay into the pure resin. Further addition of whisker and/or fibers into such base ink resulted in SiC- and SiC/C-filled inks. Adapted with permission from Compton *et al.*⁹

Reinforcement of the walls of the printed cellular structures at multiple length scales was accomplished through the addition of silicon carbide whiskers (0.65 μm in diameter; 12 μm mean length) and carbon fibers (10 μm in diameter; 220 μm mean length) into the base epoxy ink

comprising the pure resin and the nano-clay. The incorporated fibers increase both the storage and the loss moduli of the printing ink, while keeping the viscoelastic response required for the direct writing process (Figure 5D). In this exemplary system, the printed ink was consolidated through a dual curing process at 100 and 220°C. The presence of stiff fibers and whiskers is expected to significantly enhance the elastic modulus of the consolidated epoxy polymer, especially when the reinforcement is oriented parallel to the loading direction (longitudinal). This is confirmed by mechanical tests on printed tensile bars representative of the wall material (Figure 6A). The fracture surface of bars containing reinforcement aligned parallel to the loading direction (longitudinal) suggests that fiber pull-out is an active toughening mechanism in these composites. The presence of reinforcing particles increases the elastic modulus of the base epoxy to levels comparable to that of the balsa cell wall and about one order of magnitude higher than that of most commercial 3D printed polymers (see data corresponding to “tensile bars” in Figure 6C).

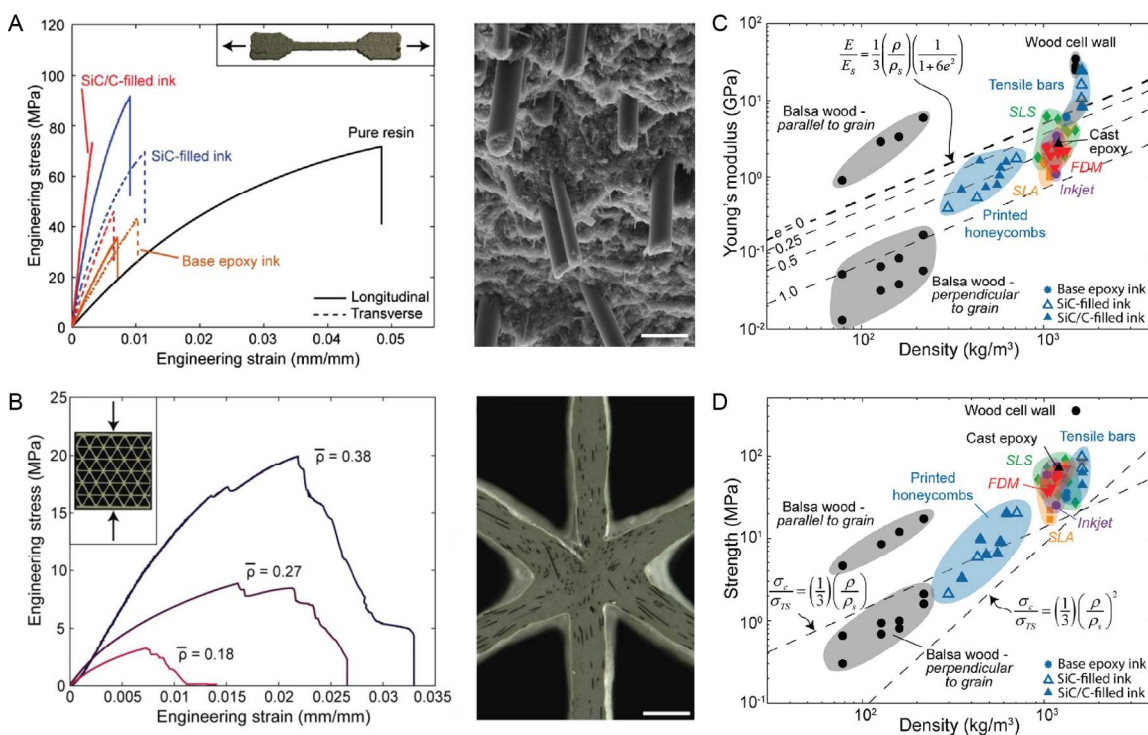


Figure 6. Mechanical behavior of epoxy-based cellular composites reinforced with silicon carbide whiskers and carbon fibers obtained via DIW.⁹ A. Tensile stress-strain curves obtained for dogbone consolidated specimens mechanically loaded in different directions (left) and a scanning electron microscopy (SEM) image depicting fibers that were pulled out from the epoxy matrix during fracture (right). Scale bar, 20 μm . B. Compressive stress-strain curves measured for

cellular composites with different relative densities ρ (left) and a SEM image showing the alignment of fibers along the printing direction (right). Scale bar, 500 μm . C,D. Ashby plots displaying the properties of printed honeycombs in comparison to balsa wood and other 3D printed polymers. Dashed lines in C indicate the theoretical relative elastic modulus (E/E_s) predicted for triangular lattices assuming different waviness of the cell wall (e). Dashed lines in D display the linear and square dependence of the relative strength (σ_c/σ_{Ts}) on the relative density (ρ/ρ_s) expected for triangular and hexagonal lattices, respectively. Adapted with permission from Compton *et al.*⁹

Direct writing of cellular structures with inks containing fibers and whiskers often leads to the alignment of reinforcement along the printing direction (Figure 5B). This results from the shear stresses developed during extrusion of the ink through the dispensing nozzle. The shear stresses responsible for the alignment effect are more pronounced close to the nozzle wall. In the exemplary system shown in Figure 6B, the nozzle diameter was sufficiently small to result in shear-induced alignment throughout the entire cross-section of the filament.

Changing the distance between the printed filaments enables easy tuning of the final density and mechanical response of the cellular scaffolds. The compressive mechanical properties of a triangular honeycomb structure with different relative densities are shown in Figure 6B in the form of stress-strain curves. The multiple load drops observed during mechanical loading of the structure arise from single rupture events within the cellular material. Such delocalized rupture events help increase the fracture energy of the scaffold.

The relative elastic modulus of the printed honeycombs (E/E_s) scales linearly with the relative density (ρ/ρ_s), as expected for triangular lattices.⁶⁵ Absolute values of E/E_s can be reasonably predicted by a simple analytical expression if the waviness of the printed cell walls (e) is taken into account (Figure 6C). The compressive strength of the printed triangular honeycombs was found to scale with the square of the relative density (Figure 6D).⁹ This contrasts with the linear dependence expected for stronger stretching-dominated triangular lattices. A scaling exponent of 2 is typical of weaker bending-dominated hexagonal lattices.⁶⁵ Rotation of nodes and elastic buckling of cell walls were indeed observed during the compression tests, confirming the bending-dominated failure of the honeycomb. This is reflected in the single rupture events depicted in Figure 6B, which resembles the failure mechanism of balsa wood in its weaker transverse direction. Nodal misalignment is the most probable reason for the onset of such failure mechanisms and the inability to reach the higher strength level predicted for triangular honeycombs. Yet, the higher density of the printed cellular structure results in absolute elastic modulus and strength comparable to that of lighter balsa wood loaded along the stronger longitudinal direction.

Although the orientation of stiff particles in the printing direction enhances properties and functionalities of materials printed by DIW as compared to unreinforced counterparts, further control over the orientation of anisotropic particles would be required to replicate the exquisite fiber architectures and functionalities of plants and mineralized biological materials (Figure 1). Particle alignment control independent of the printing direction should enable reinforcement in any deliberate orientation, greatly enhancing the design space of bioinspired architectures. As discussed below, the combination of AM technologies with magnetically-assisted orientation control offers an interesting approach in this direction.

3D Magnetic Printing

The use of magnetic fields to control the orientation of anisotropic particles within a printed object has been recently demonstrated in two independent, complementary studies.^{11, 13} In one of the resulting technologies, magnetic orientation control is implemented in a stereolithography printing platform.¹¹ Stereolithography is one of the most widely used technologies for the additive manufacturing of polymer parts.^{66, 67} This well-established approach relies on the layer-by-layer polymerization of a fluid reactive mixture of monomers/oligomers and photoinitiators placed in a resin container (Figure 7A). Polymerization is accomplished by illuminating a thin layer of the reactive mixture positioned between the surface of the building plate and the bottom of the resin container. In projection mode, the shape of the fabricated part is defined by illuminating a specific area of the resin layer using a digital light processor placed beneath the printer. After polymerization of this well-defined area, the build plate is pulled upwards to allow for spreading of a new layer of liquid resin, initiating a new cycle of the process. In a recently developed technique named continuous liquid interface production (CLIP), an oxygen permeable bottom plate is used to prevent polymerization at the resin-plate interface, significantly accelerating the manufacturing speed.⁶⁸

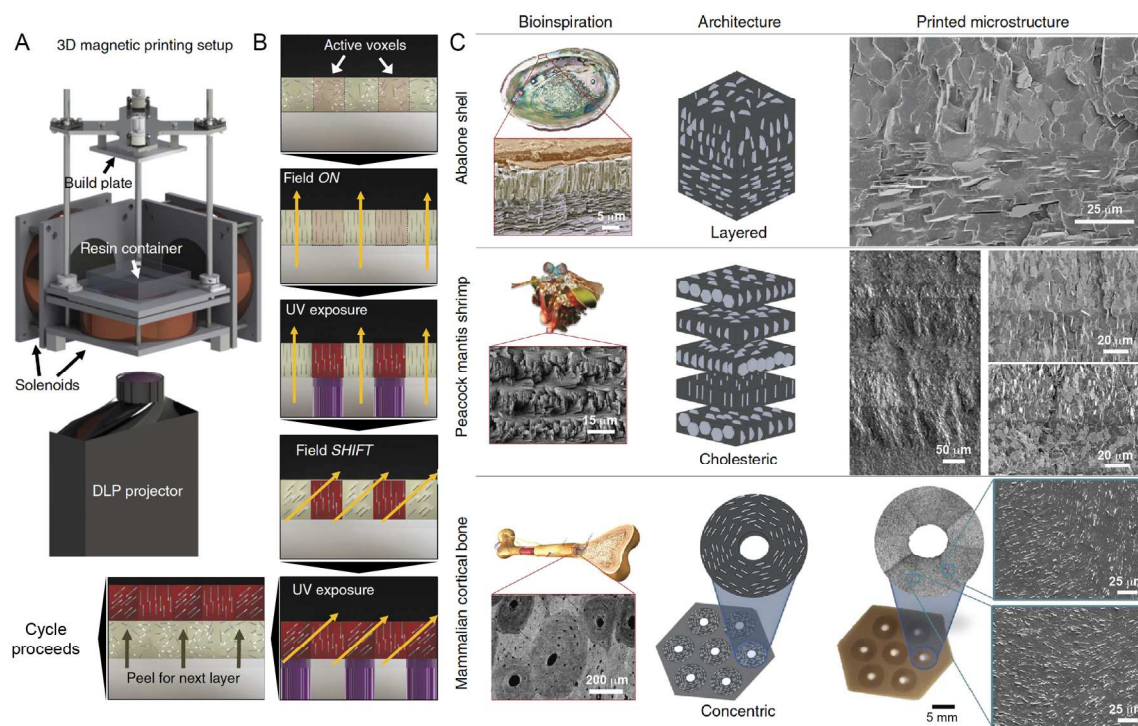


Figure 7. 3D Magnetic Printing technology and bioinspired composite architectures fabricated by exploiting the voxel-based particle orientation control.¹¹ A. Stereolithography platform equipped with solenoids to magnetically control particle orientation. B. Workflow outlining the main steps required to achieve particle orientation control within individual voxels. C. Examples of exquisite biological architectures and bioinspired synthetic counterparts produced via 3D Magnetic Printing. Adapted with permission from Martin *et al.*¹¹

The incorporation of filler particles inside the liquid resin makes it possible to also additive manufacture polymer-based composites using stereolithography.⁶⁹ Taking advantage of this feature, a SLA platform was developed to fabricate polymer-based composites with reinforcement orientation control inspired by the exquisite architectures of biological materials (Figure 1).¹¹ Orientation control is achieved by suspending anisotropic particles exhibiting ultra-high magnetic response (UHMR) within the reactive resin.⁷⁰ For non-magnetic filler materials, UHMR is achieved by decorating the anisotropic particles with superparamagnetic iron oxide nanoparticles (SPIONs) through electrostatic adsorption, in-situ particle formation or selective droplet wetting approaches.⁷⁰⁻⁷² The use of anisotropic particles with sizes ranging typically from 5 to 10 μm results in ultra-high magnetic response using SPION concentrations as low as 0.01 vol%.⁷⁰ Because particles in this size range are too large to be strongly affected by Brownian motion and too small to be dominated by gravity, magnetic fields in the order of only 1-10 milliTeslas are needed for orientation control.

Orientation control of UHMR particles was implemented in an additive manufacturing process by equipping a standard SLA platform with three electromagnetic coils, as schematically shown in Figure 7. The new technology, referred to as 3D Magnetic Printing, allows for programming of the orientation of the UHMR anisotropic particles at an individual voxel level.¹¹ This is realized through the introduction of two additional steps within a standard SLA manufacturing protocol (Figure 7B). First, a rotating magnetic field is applied to align the UHMR particles in a specific direction within the liquid resin layer.^{73, 74} Second, the resin layer is illuminated only in those voxels where the imposed particle orientation is desired. These two steps are sequentially repeated until all the pre-programmed orientations are implemented in the polymer layer. The process then continues by lifting the build plate to allow for spreading of the next resin layer. An attractive feature of this technology is that it enables full voxel-based control of particle orientation combined with the high resolution offered by stereolithography. To demonstrate the potential of this approach, composite architectures that resemble the structural motifs found in bone, mollusk shells and in the dactyl club of the mantis shrimp were successfully created using 3D Magnetic Printing (Figure 7C).

Composites with locally programmable reinforcement architectures lead to functionalities that are not accessible using homogeneous monoliths or conventional long fiber reinforced structures. As illustrative examples, architectures were programmed and printed to exhibit a locally harder area on a composite surface or to steer the path of a propagating crack (Figure 8). Importantly, such new functionalities arise simply by controlling the orientation of anisotropic particles in individual voxels, while keeping the chemical composition constant throughout the entire composite. The key design principle resulting in local hardening and crack steering is the fact that the particle orientation can either strengthen or weaken individual voxels depending whether the alignment is parallel or perpendicular to the loading direction, respectively (Figure 8A).

The composite part shown in Figure 8B,C demonstrates the potential of 3D Magnetic Printing in creating surfaces with a hardness pattern programmed through voxel-specific particle alignment control.¹¹ Areas containing out-of-plane aligned stiff platelets exhibit hardness levels that are 30-40% higher than that of areas containing in-plane oriented platelets. A sharp transition is observed between harder and softer areas, indicating that the hardness level can be resolved down to individual voxel sizes.

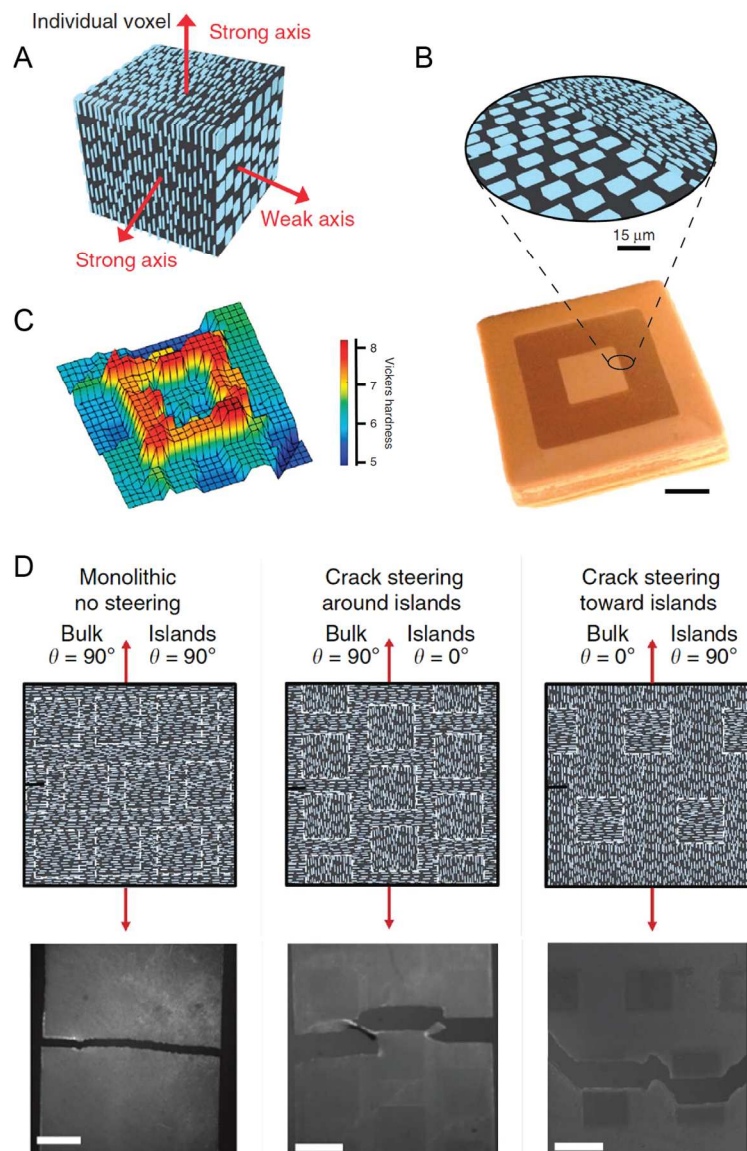


Figure 8. Synthetic composites fabricated via 3D Magnetic Printing exhibiting reinforcement architectures that locally harden the surface or can steer the path of a propagating crack.¹¹ A. The anisotropic mechanical response of an individual voxel with well-defined platelet orientation. B. Printed composite block displaying distinct particle orientations at the surface. Scale bar, 4 mm. C. Hardness map of the composite surface, indicating site-specific hardening through platelet orientation control. D. Composites with islands exhibiting particle orientation orthogonal to that of the bulk matrix to either attract or deflect propagating cracks. Scale bar, 4mm. Adapted with permission from Martin *et al.*¹¹

The effect of locally distinct particle orientations on the path of a crack propagating throughout a printed composite is shown in Figure 8D. In this case, composites with squared

islands displaying a distinct particle orientation with respect to the surrounding bulk matrix were printed and compared to a homogeneous specimen with uniform particle alignment throughout. Fracturing of such architectures reveals that cracks are attracted to islands displaying particle orientation parallel to the propagation direction, whereas islands with particle orientations perpendicular to the main crack tend to deflect it and generate a more tortuous path (Figure 8D). Such programmed crack-microstructure interactions offer an interesting strategy to tailor the fracture behavior of composite materials, similarly to a laser engraving approach recently demonstrated in glass.⁷⁵

Although the voxel-specific control of particle orientation provided by 3D Magnetic Printing opens many new possibilities for the design of complex composite architectures, tailoring the local chemical composition of the printed material using this approach has not yet been demonstrated. In the current system the chemistry of the printed material is defined by the monomer composition in the large resin bath used in the process. Future development of the technique to allow for easy exchange of the printing monomer composition might address this limitation. Combining continuous liquid interface production (CLIP) with UHMR particles designed for quick magnetic alignment is also an interesting avenue to be pursued.

Multimaterial Magnetically-assisted 3D Printing (MM-3D Printing)

The magnetic manipulation of anisotropic particles has also been recently implemented in a direct ink writing (DIW) platform to enable the fabrication of intricate 3D composite architectures that combine particle orientation control with multi-material capabilities.¹³ The new technology, named Multimaterial Magnetically-assisted 3D Printing (MM-3D Printing), offers the flexibility of extrusion-based methods with the microstructural control accessible through magnetic directed assembly of particles. In MM-3D Printing, multiple materials can be printed by simply loading distinct syringes with inks containing different monomer compositions and particle concentrations (Figure 9A). Continuous gradients in composition are also possible if mixing units are used before the extrusion nozzle. Magnetic control is achieved by introducing UHMR particles into the DIW ink and equipping a conventional extrusion-based printer with a magnet or a set of electromagnetic coils.

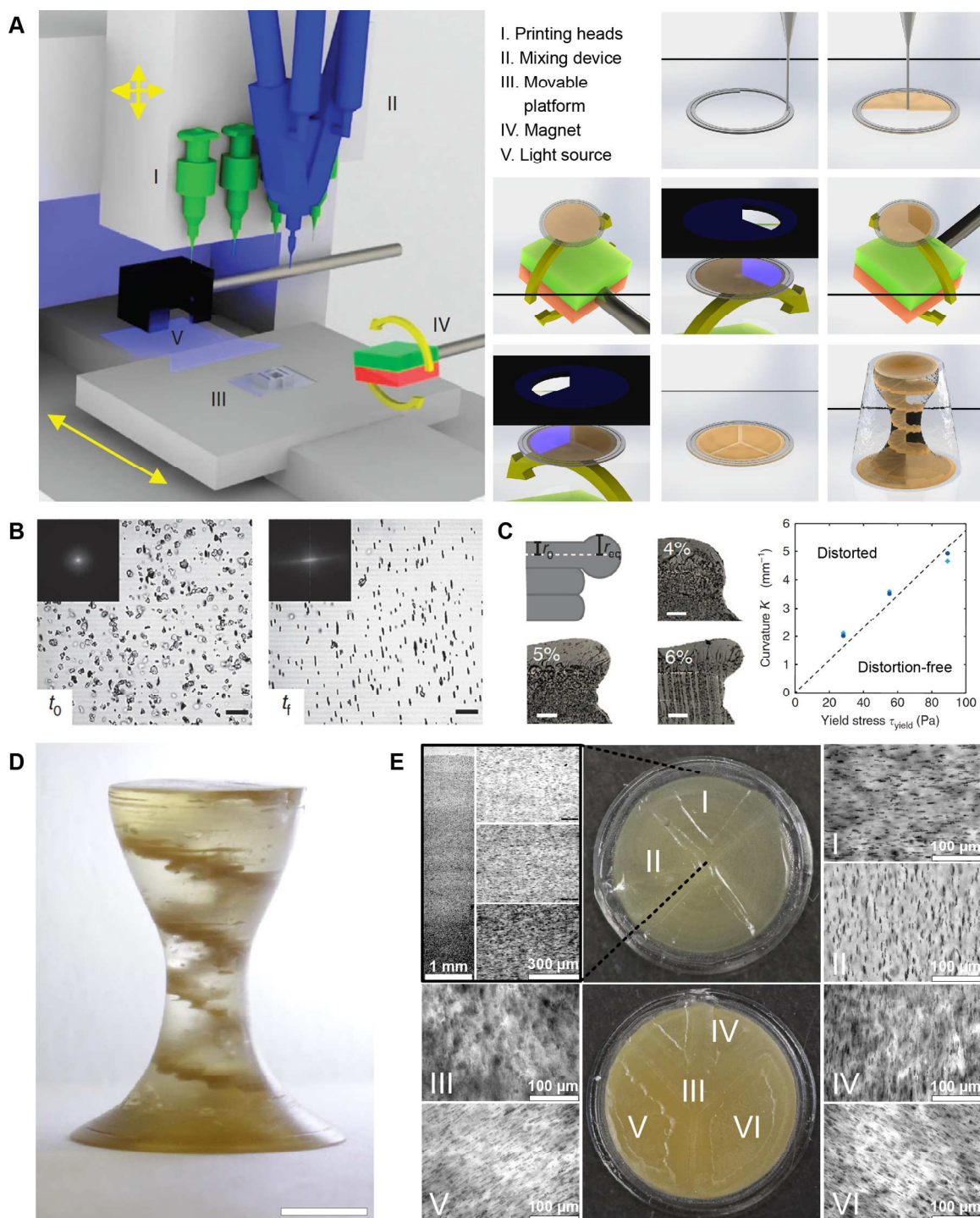


Figure 9. MM-3D Printing technology and an exemplary exquisite composite architecture that can be generated using multi-material capabilities and voxel-based particle orientation control.¹³ A. Direct ink writing setup equipped with a magnet and multiple cartridges (left), and typical workflow of the magnetically-assisted printing process (right). B. Biaxial magnetic alignment of UHMR platelets suspended in a texturing ink (time $t_f \approx 1$ min). Scale bar, 50 μm . C. Shape of overhangs

obtained with a shaping ink containing different concentrations of a rheology modifier (left) and the rheological response required to generate distortion-free filaments (right). Scale bar, 200 μm . D. MM-3D printed object with internal helicoidal staircase made by controlling the distribution and local orientation of stiff platelets. Scale bar, 5 mm. E. Detailed features of the top (upper images) and the bottom (lower images) of the printed object, illustrating the precise control over local platelet concentration and orientation. Adapted with permission from Kokkinis *et al.*¹³

Two sets of inks are typically required to print three-dimensional objects using MM-3D Printing.¹³ A low-viscosity “texturing ink” containing UHMR particles is used to achieve local orientation control, whereas a “shaping ink” loaded with a rheological modifier is utilized to ensure that the printed material retains its shape after deposition. Texturing inks with a Newtonian rheological behavior and viscosity lower than 0.2 Pa.s enables alignment of particles using a low magnetic field of 40 mT in a timescale around 1 minute (Figure 9B). The ultra-high magnetic response of the particles⁷⁰ is key for the technology, since it enables orientation control using small, compact magnets that can be easily coupled to a standard 3D printer. Shape retention is ensured by formulating a non-Newtonian shaping ink that exhibits a yield stress sufficiently high to prevent the geometrical distortion of deposited filaments. Local shape distortion is often driven by capillary stresses acting across curved surfaces along the printed material. Such capillary stress (ΔP) scales linearly with the interfacial tension γ and the curvature of the surface κ , such that: $\Delta P = \kappa\gamma$. By equating capillary and yield stresses, one can thus estimate the minimum yield stress required to generate a distortion-free curvature for an ink of known surface tension (Figure 9C). A convenient way to tune the yield stress of the ink is through the addition of fumed silica (FS) as rheology modifier. For the ink system shown in Figure 9, a FS concentration of 8 wt% leads to an yield stress of 160 Pa, allowing for the deposition of distortion-free filaments with radii of curvature ($1/\kappa$) approaching 100 μm .

The steps involved in the layer-by-layer fabrication of a 3D object using shaping and texturing inks in a MM-3D Printing platform are schematically depicted in Figure 9A.¹³ First, a shaping ink is printed to establish the contour of the 3D geometry desired. Afterwards, a texturing ink is deposited within the contours defined by the shaping ink. A rotating magnetic field is then applied to deliberately align UHMR fibers and/or platelets suspended in the deposited texturing ink.^{73,74} Positions within the layer that are programmed to exhibit the imposed particle orientation are selectively polymerized via exposure to UV or blue light. Selective polymerization has been demonstrated using patterned masks, but can also be accomplished using stereolithographically projected light. Alike 3D Magnetic Printing, this allows for voxel-specific orientation control. The alignment and selective polymerization steps are sequentially repeated until all the voxels within the deposited material are textured and consolidated. The process continues by the deposition of new layers of shaping and texturing inks until the entire object is printed.

An exemplary 3D object is shown in Figure 9D to demonstrate the potential of MM-3D Printing in fabricating composite parts with unprecedented complex architectures.¹³ The object has the form of a chalice with an external surface that continuously changes from concave to convex from bottom to top. A 3D rotating staircase structure comprising alumina platelets dispersed in an acrylate-based polymer is embedded within the object, forming a helix whose radius is defined by the outer contour of the chalice. Platelets within each step of the staircase are programmed to align alternately either radially or tangentially with respect to the object surface. Because it is platelet-free, the embedding phase surrounding the staircase is transparent. The top surface of the object was programmed to display a concentration gradient of tangentially aligned platelets, whereas the bottom surface is designed to show a well-defined motif with different local orientations of platelets at the same overall concentration (Figure 9E). This level of control over the composite microstructure finds no parallels among man-made materials and is only rivaled by the exquisite architectures encountered in biological systems (Figure 1).

Taking advantage of the vast design space accessible by programming the local composition and particle orientation of composites, living organisms exploit microstructural control to produce biological materials with remarkable mechanical behavior, shape-changing capabilities and optical properties.^{18, 21, 22, 76} The potential of MM-3D Printing in exploring this ample design space to generate functional parts was demonstrated by printing load-bearing 3D objects that are able to self-shape upon an external stimulus (Figure 10).¹³ In the exemplary cuboid object shown in Figure 10A, bilayers made from polymers with different swelling properties were printed along the height of the object to make the cuboid walls autonomously change their surface curvature from a flat to concave or convex when exposed to a swelling liquid. Independently from the shape change programmed through the polymer composition, the orientation of platelets was tuned to locally adjust the stiffness and the swelling of the cuboid wall (Figure 10A,B). In another example (Figure 10C,D), two separate parts with complementary key-lock geometries were designed to undergo an autonomous shape change that increases their interlocking when exposed to a solvent. Similarly to the cuboid, different polymer compositions were used to program the shape change, whereas particles were oriented parallel to the walls to provide local mechanical reinforcement. In the interlocked state, these exemplary objects are able to carry loads much heavier than their own weight (Figure 10D). Besides solvent-induced swelling, the chemistry of the printed polymer can also be designed to enable the use of other actuation triggers, including temperature, pH changes, electrical current or air pressure.⁷⁷ Such autonomously actuated composites may find applications in soft robotics and biomedical devices, shape-changing architectural elements or morphing structures in airplanes and vehicles.

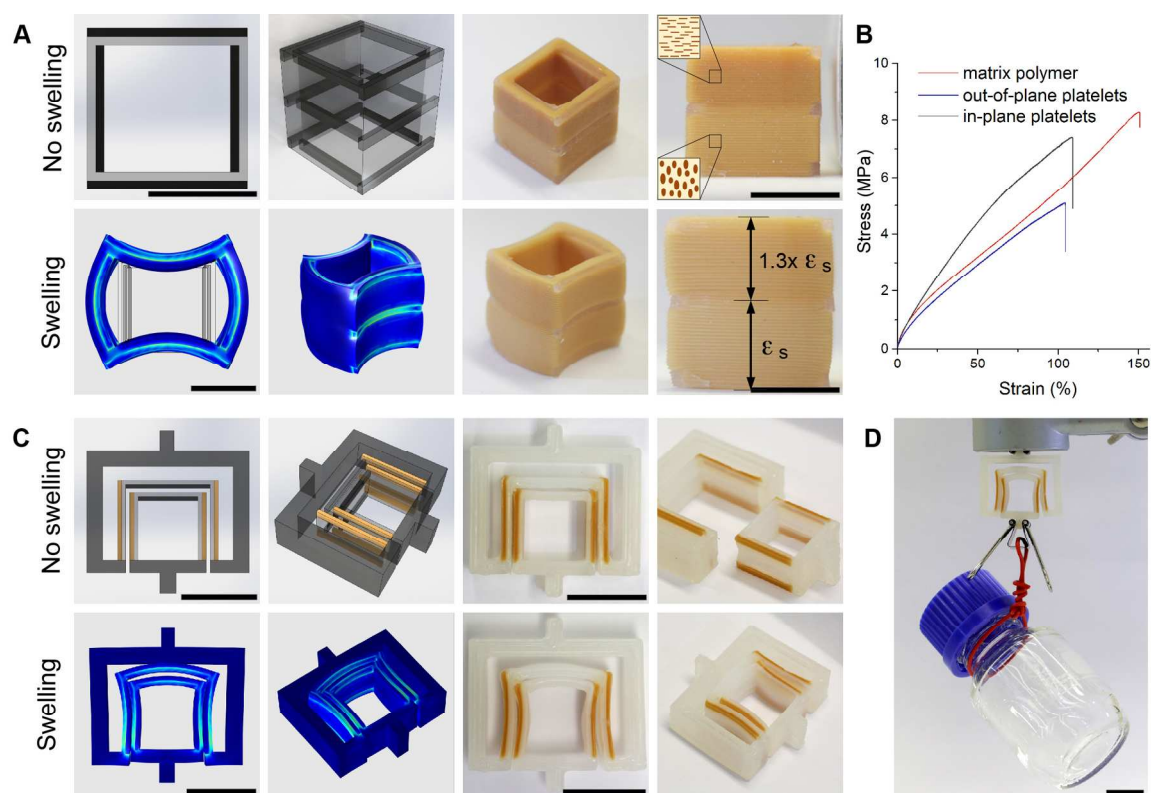


Figure 10. Self-shaping soft objects with load-bearing capability fabricated by MM-3D Printing.¹³ A. Cuboid printed using soft (light grey) and stiff (dark grey) polymers combined with distinct platelet orientations before (upper images) and after (lower images) a swelling-induced shape change. Scale bars, 10 mm. B. Effect of platelet orientation on the mechanical behavior of the printed polymer. C. Soft objects with complementary key-lock geometries whose local material composition was programmed to enable a shape change into a mechanically interlocked state. Scale bars, 15 mm. D. Load bearing capability of the key-lock soft objects locally reinforced with deliberately oriented alumina platelets (in brown). Scale bar, 15 mm. Overall, drawings shown in grey/black represent the designed geometries, whereas blue-colored representations indicate the simulated geometries after the shape change. Adapted with permission from Kokkinis *et al.*¹³

Despite their unique capability to design the composite particle architecture at the individual voxel level, current magnetically-assisted direct ink writing and stereolithography approaches are limited in terms of the concentration of particles that can be incorporated in the monomers. Relatively low volume fraction of particles (< 15 vol%) is needed to make the resin and monomers sufficiently fluid for spreading and extrusion, while minimizing clogging issues inside the nozzle or resin bath. In extrusion-based processes, printing formulations exhibit low-shear viscosity typically lower than 10^3 Pa.s.¹³ Much lower viscosities are needed to ensure resin

spreading in stereolithographic processes. High particle volume fractions inevitably increase the viscosity level beyond these upper limits. Although future development of these techniques might extend further the upper limit in filler concentration, alternative approaches have been pursued to obtain complex composite architectures with higher volume fraction of particles and thus enhanced mechanical performance.

Magnetically-assisted slip casting (MASC)

Magnetically-assisted slip casting (MASC) is a recently developed additive manufacturing technology that offers a simple and cost-effective route for the fabrication of complex-shaped objects containing high concentrations of particles with deliberate orientation control. The method combines a traditional ceramic manufacturing process to deposit particles in an additive layer-by-layer fashion (slip casting)⁷⁸ with an advanced magnetically-assisted technology to control the orientation of such particles during deposition.⁷⁰

The layer-by-layer deposition process, known as slip casting, consists in simply pouring a fluid suspension of particles into a complex-shaped porous mold (Figure 11A).⁷⁹ Gypsum (plaster of Paris) is the most common material used as porous mold. Because the mold material is wettable by the liquid phase of the suspension, a curved air-liquid meniscus readily develops within the pores of the mold. Such curved meniscus gives rise to a capillary force that pulls the liquid from the suspension into the mold's internal porosity. The pore sizes in dry gypsum range typically from 0.5 to 6 μm .⁸⁰ Suspended particles larger than the mold's pores accumulate and eventually jam next to the wall of the mold forming a so-called cake. A cake is formed even if the suspension contains particles smaller than the pore sizes. In this case, clogging of the mold's pores with such fine particles gives rise to smaller interstices/pores that ensure jamming and accumulation of all suspended particles at the mold wall. Regardless of the size of suspended particles, the cake thickness increases non-linearly with time, creating a well-defined advancing jamming front (Figure 11B).⁸¹⁻⁸³ The additive nature of the process lies on the fact that the formulation of the suspension can be changed during casting to generate lamella with different compositions.

In MASC, a magnetic field is applied to the suspension during the slip casting process in order to control the orientation of particles while they are freely movable in the fluid state.^{73, 74} Eventually, the particle orientation defined by the imposed magnetic field is fixed within the cake structure as the jamming front advances away from the surface of the mold. Thus, if the cake growth kinetics is known, the direction of the magnetic field can be deliberately changed in time to generate a cake with any desired particle orientation pattern (Figure 11B).

The level of microstructural control achievable with MASC can be illustrated by the bio-inspired architecture with periodic particle orientation shown in Figure 11C. In this example, stiff platelets were assembled in a specific orientation pattern by changing the angle of the applied magnetic field relative to the mold in a stepwise manner until multiple rotations of the magnet were completed. The time τ spent at each step was varied in different experimental runs to generate structures with platelet orientation patterns with well-defined distinct pitches (Figure 11B). Remarkably, the pitch of the resulting architectures closely followed the values predicted by simply correlating the periodic change in the magnetic field direction with the growth kinetics of the jamming front. The periodic structure obtained is conceptually similar to the fiber plywood architecture found in several biological materials, including fish scales,⁸⁴ the cell walls of plants,⁸⁵ exoskeletons of lobsters⁸⁶ and the dactyl club of stomatopods.⁸⁷ Importantly, the use of microplatelets as reinforcing building blocks enables the fabrication of plywood periodic structures at much smaller length scales compared to those achieved thus far using conventional composite processing technologies.^{88, 89} The ample freedom in deliberately controlling the orientation of reinforcing particles in a continuous layer-by-layer fashion makes it possible to replicate any of the structural motifs depicted in Figure 1. Combining different motifs, including for example the prismatic and the plywood arrangements of the outer and inner layers of the dactyl club,^{90, 91} becomes straightforward with MASC.

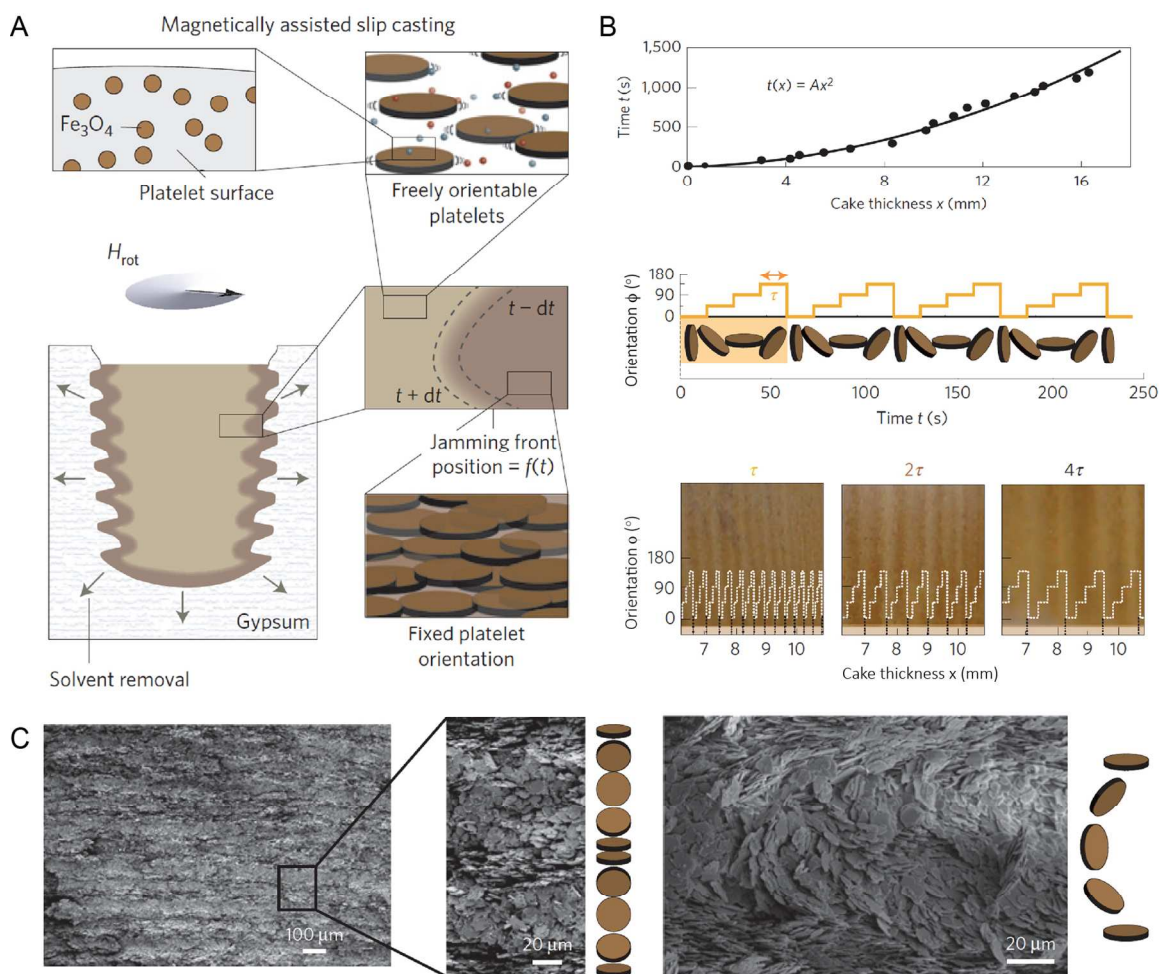


Figure 11. Magnetically-assisted Slip Casting (MASC) technology and exemplary periodic architectures that can be created featuring high volume fraction of oriented anisotropic particles.¹² A. Schematics of the slip casting process that is combined with transient magnetic fields to control the local orientation of UHMR particles within the consolidated material (dark brown). B. Dynamics of the casting process (upper row) and of the imposed magnetic field orientation (middle row), which are used to program the local texture within the manufactured object (bottom row). C. Examples of periodic architectures created via MASC by aligning high concentrations of platelets in continuously changing orientations. Adapted with permission from Le Ferrand *et al.*¹²

To create bio-inspired composites with a high concentration of deliberately aligned particles, the structures generated by MASC are further processed using pressing and sintering protocols normally utilized in ceramic processing to increase the density of particle compacts (Figure 12A,B).⁷⁹ Taking the nacre-like architecture as an illustrative example, well-established cold or hot pressing processes allow tuning of the volume fraction of alumina platelets in a brick-and-mortar design from 30% up to a remarkable level of nearly 100%. The alumina bricks in this

case are interconnected via “mineral bridges” formed by partial sintering of nanoparticles initially added to the casting suspension. The high level of mineralization achieved leads to nacre-like alumina parts in the form of 5cm-diameter disks with outstanding mechanical properties. The average fracture strength of such parts is comparable with that of the strongest commercial aluminas (650 MPa), whereas the fracture toughness increases during crack propagation to a level that is 3 to 4-fold higher than typical values for alumina (Figure 12C). Alternatively to fully-mineralized parts, brick-and-mortar structures with lower volume fractions of inorganic platelets can be produced to allow for the creation of a softer polymer matrix through the polymerization of infiltrated monomers. Relative to the pure polymer, the resulting polymer-based nacre-like composite shows a 7 to 10 times higher fracture toughness combined with 3 to 4-fold improved tensile strength. In yet another example, ceramic platelets have also been mixed with metal flakes during MASC to produce functional nacre-like composites combining high specific strength and high electrical and thermal conductivity (Figure 12C).

The full potential of MASC in generating bio-inspired materials with intricate architectures was demonstrated by fabricating a complex-shaped synthetic tooth that contains an enamel-dentin bilayer structure with different local chemical composition and reinforcement orientation.¹² The synthetic tooth was obtained by sequential casting of two different suspensions into a porous gypsum mold made as an imprint from a human molar tooth. Figure 12D confirms the suitability of slip casting in replicating the finest details of the complex geometry of the natural molar tooth. The outer enamel layer was made chemically different from the inner dentin layer by adding silica nanoparticles to the first casting suspension, which enables stronger densification of the MASCed structure during the sintering step. In addition to the local chemistry, alumina platelets were magnetically aligned perpendicular and parallel to the surface of the mold to replicate the orientation design of the enamel and dentin layers of natural tooth, respectively. As evidenced by elemental analysis, SEM images and microindentation measurements (Figure 12E), the presence of silica and perpendicularly aligned platelets led to a synthetic enamel that is significantly denser and harder than the inner dentin layer. The final hardness profile across the enamel/dentin-like layers of the synthetic tooth qualitatively resembles the local properties of the biological counterpart (Figure 12E).

Because it is a particle-based process, MASC is especially suited for the fabrication of bioinspired materials with the very high volume fractions of particles needed to reach outstanding mechanical properties. However, applications requiring control of the local composition and particle orientation at the single voxel level do not benefit from the lamellar architecture of the materials produced by MASC. Moreover, other methods that would allow for the incorporation of a second continuous phase without the need of an infiltration step would further increase the versatility of the MASC process.

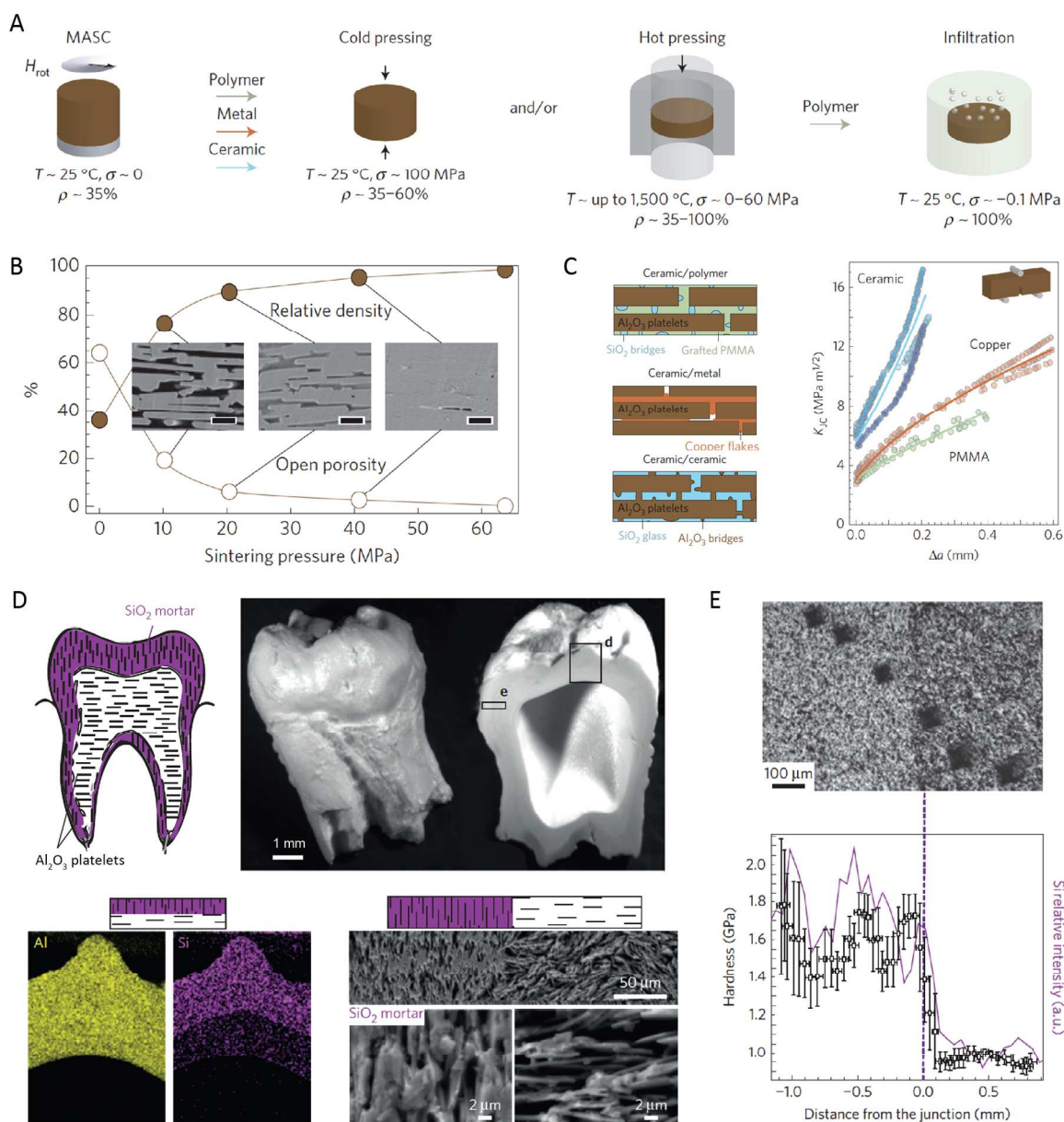


Figure 12. Nacre-like functional composites and a microstructured synthetic tooth obtained by further processing of MASC scaffolds.¹² **A.** Workflow used to create nacre-like composites with high volume fraction of platelets and tunable matrix composition. **B.** Volume fraction of platelets in the nacre-like composites as a function of the pressure applied during sintering at 1400 °C of the MASC scaffolds. **C.** Examples of MASC-derived nacre-like composites with ceramic, polymer or metal functional matrices and their increasing crack growth resistance. **D.** Tooth-shaped object exhibiting a bilayer structure with locally tuned composition and platelet orientation inspired by the architecture of biological tooth. **E.** Hardness profile across the bilayer, showing the agreement between the local mechanics of the composite and the site-specific composition and texture within the object. Adapted with permission from Le Ferrand *et al.*¹²

Summary and outlook

Additive manufacturing provides opportunities to design the microstructure of materials at levels that have so far only been accessible by living organisms in nature. This design flexibility has recently started to be exploited to fabricate composite parts with enticing biologically-inspired architectures, such as brick-and-mortar patterns, reinforced periodic lattices, mechanically graded 3D geometries, well-defined surface topographies, rotating plywood designs and multilayered structures. A variety of established and novel additive manufacturing technologies have been utilized to create these architectures, including PolyJet Printing, Direct Ink Writing (DIW), 3D Magnetic Printing, Multimaterial Magnetically-assisted 3D Printing (MM-3D Printing) and Magnetically-Assisted Slip Casting (MASC). Each of these technologies features advantages and drawbacks, which should be considered when selecting the most suitable manufacturing process for the bio-inspired material of interest.

Importantly, the design space covered by such additive manufacturing technologies extends beyond the unique 3D shaping capabilities of conventional rapid prototyping to include also local control over the material composition and the orientation of constituent building blocks. Although design flexibility is a highly desirable feature for accessing a wide range of properties and functionalities, it also makes the identification of optimal architectures more challenging. In this context, additive manufacturing methods can greatly benefit and also contribute to biomimetic materials research. On one hand, design principles derived from the investigation of biological materials can guide the identification of interesting composite architectures. On the other hand, bio-inspired composites fabricated through additive manufacturing can serve as tunable model systems to deepen our understanding of biological design principles and adapt natural architectures to the boundary conditions of engineering applications. In addition to the examples presented here, bioinspired AM materials have already been utilized as model systems to investigate fundamental design concepts of nacre and chiton teeth.^{48, 92}

By enabling unparalleled microstructural control, additive manufacturing of bioinspired composites sets a new paradigm in the design and fabrication of functional materials. Functionalities are no longer dictated only by the chemical composition of the building blocks that constitute state-of-the-art homogeneous materials. Instead, graded and textured heterogeneous architectures can be designed to meet the functional demands of specific applications, enabling improvement in performance or reaching adequate response using more sustainable or biocompatible building blocks.

Much work is yet to be accomplished before these exciting new possibilities for materials design and fabrication are fully explored. Future research efforts may be dedicated to (i)

identifying and extending current limits of additive manufacturing technologies to more closely replicate the rich variety of complex biological architectures; (ii) developing strategies to implement hierarchical organization in printed parts; (iii) designing heterogeneous composite materials that are locally tuned to fulfill the functional demands of specific environments and applications, (iv) structuring sustainable and biocompatible building blocks into strong and flaw-tolerant architectures and (v) utilizing additive manufactured composites as model systems to investigate structure-property relationships in bioinspired and biological materials. Further studies along these and related research directions are expected to consolidate the merger of additive manufacturing and biological design principles as an effective, paradigm-shifting pathway towards the design and fabrication of next-generation functional composite materials.

Acknowledgements

I am grateful to the financial support of the Swiss National Science Foundation through the awarded Consolidator Grant (BSCGI0_157696) and the Swiss National Center of Competence in Research (NCCR) for Bio-Inspired Materials. Special thanks also to my current and former co-workers and students who have contributed to the development of bioinspired composites at the Complex Materials group at ETH Zurich. Finally, I acknowledge Dr. Daniel Dikovskiy for kindly providing one of the images displayed in the manuscript.

References

1. P. Calvert and R. Crockett, *Chem. Mater.*, 1997, **9**, 650-663.
2. G. Villar, A. D. Graham and H. Bayley, *Science*, 2013, **340**, 48-52.
3. M. Fantini, F. de Crescenzo, F. Persiani, S. Benazzi and G. Gruppioni, *Rapid Prototyping J.*, 2008, **14**, 318-324.
4. N. Oxman, E. Tsai and M. Firstenberg, *Virtual Phys. Prototyp.*, 2012, **7**, 261-274.
5. E. Lloret, A. R. Shahab, M. Linus, R. J. Flatt, F. Gramazio, M. Kohler and S. Langenberg, *Comput. Aided Des.*, 2015, **60**, 40-49.

6. J. Klein, M. Stern, G. Franchin, M. Kayser, C. Inamura, S. Dave, J. C. Weaver, P. Houk, P. Colombo, M. Yang and O. N., *3D Printing and Additive Manufacturing*, 2015, **2**, 92-105.
7. J. Stampfl, H. E. Pettermann and R. Liska, in *Biomimetics -- Materials, Structures and Processes*, eds. P. Gruber, D. Bruckner, C. Hellmich, H.-B. Schmiedmayer, H. Stachelberger and I. C. Gebeshuber, Springer Berlin Heidelberg, 2011, DOI: 10.1007/978-3-642-11934-7_6, ch. 6, pp. 105-123.
8. Q. A. Fu, E. Saiz and A. P. Tomsia, *Adv. Funct. Mater.*, 2011, **21**, 1058-1063.
9. B. G. Compton and J. A. Lewis, *Adv. Mater.*, 2014, **26**, 5930-5935.
10. L. S. Dimas, G. H. Bratzel, I. Eylon and M. J. Buehler, *Adv. Funct. Mater.*, 2013, **23**, 4629-4638.
11. J. J. Martin, B. E. Fiore and R. M. Erb, *Nat. Commun.*, 2015, **6**, Article number 8641.
12. H. Le Ferrand, F. Bouville, T. P. Niebel and A. R. Studart, *Nat. Mater.*, 2015, **14**, 1172-1179.
13. D. Kokkinis, M. Schaffner and A. R. Studart, *Nat. Commun.*, 2015, **6**, Article number 8643.
14. A. R. Studart, *Adv. Funct. Mater.*, 2013, **23**, 4423-4436.
15. A. R. Studart, *Adv. Mater.*, 2012, **24**, 5024-5044.
16. A. R. Studart, R. Libanori and R. M. Erb, in *Materials Design Inspired by Nature: Function through inner architecture*, eds. P. Fratzl, J. Dunlop and W. R., RSC Publishing, 2013, ch. 15, pp. 322-358.
17. S. Thomopoulos, V. Birman and G. M. Genin, *Structural Interfaces and Attachments in Biology*, Springer New York, 2013.
18. J. W. C. Dunlop and P. Fratzl, *Annu. Rev. Mater. Res.*, 2010, **40**, 1-24.

19. P. Fratzl and R. Weinkamer, *Prog. Mater. Sci.*, 2007, **52**, 1263-1334.
20. H. D. Espinosa, J. E. Rim, F. Barthelat and M. J. Buehler, *Prog. Mater. Sci.*, 2009, **54**, 1059-1100.
21. M. A. Meyers, P. Y. Chen, A. Y. M. Lin and Y. Seki, *Prog. Mater. Sci.*, 2008, **53**, 1-206.
22. M. A. Meyers, J. McKittrick and P.-Y. Chen, *Science*, 2013, **339**, 773-779.
23. B. Pokroy and E. Zolotoyabko, *J. Mater. Chem.*, 2003, **13**, 682-688.
24. F. Barthelat, H. Tang, P. D. Zavattieri, C. M. Li and H. D. Espinosa, *J. Mech. Phys. Solids*, 2007, **55**, 306-337.
25. N. Kroger, *Science*, 2009, **325**, 1351-1352.
26. https://commons.wikimedia.org/wiki/File:Homarus_americanus.png.
27. H. O. Fabritius, C. Sachs, P. R. Triguero and D. Roobe, *Adv. Mater.*, 2009, **21**, 391-400.
28. https://commons.wikimedia.org/wiki/File:Left_tibia_-_close_up_-_anterior_view.png.
29. S. Weiner, W. Traub and H. D. Wagner, *J. Struct. Biol.*, 1999, **126**, 241-255.
30. https://commons.wikimedia.org/wiki/File:Ochroma_pyramidale_Costa_Rica_1.jpg.
31. M. Borrega, P. Ahvenainen, R. Serimaa and L. Gibson, *Wood Sci. Technol.*, 2015, **49**, 403-420.
32. S. Weiner and L. Addadi, in *Annu. Rev. Mater. Res.*, Vol 41, eds. D. R. Clarke and P. Fratzl, 2011, vol. 41, pp. 21-40.
33. U. G. K. Wegst, H. Bai, E. Saiz, A. P. Tomsia and R. O. Ritchie, *Nat. Mater.*, 2015, **14**, 23-36.
34. L. S. Dimas and M. J. Buehler, *Soft Matter*, 2014, **10**, 4436-4442.

35. L. Guiducci, J. C. Weaver, Y. J. M. Brechet, P. Fratzl and J. W. C. Dunlop, *Adv. Mater. Interf.*, 2015, **2**.
36. S. Araya, K. Zolotovskiy, F. Veliz, J. H. Song, S. Reichert, M. C. Boyce and C. Ortiz, presented in part at the International Conference on Education and research in Computer Aided Architectural Design in Europe, Delft, The Netherlands, September 18-20, 2013 2013.
37. N. W. Bartlett, M. T. Tolley, J. T. B. Overvelde, J. C. Weaver, B. Mosadegh, K. Bertoldi, G. M. Whitesides and R. J. Wood, *Science*, 2015, **349**, 161-165.
38. L. Wen, J. C. Weaver and G. V. Lauder, *J. Exp. Biol.*, 2014, **217**, 1656-1666.
39. L. Wen, J. C. Weaver, P. J. M. Thornycroft and G. V. Lauder, *Bioinspir. Biomim.*, 2015, **10**, 066010.
40. R. O. Ritchie, *Nat. Mater.*, 2011.
41. D. Hull and T. W. Clyne, *An Introduction to Composite Materials*, Cambridge University Press, Cambridge, UK, 1996.
42. T. W. Chou, *Microstructural design of fiber composites*, Cambridge University Press, Cambridge, UK, 1992.
43. K. S. Toomey, N. R. Sottos, J. A. Lewis, J. S. Moore and S. R. White, *Nat. Mater.*, 2007, **6**, 581-585.
44. S. P. Kotha, Y. Li and N. Guzelsu, *J. Mater. Sci.*, 2001, **36**, 2001-2007.
45. A. P. Jackson, J. F. V. Vincent and R. M. Turner, *Proc. R. Soc. Lond. B Biol. Sci.*, 1988, **234**, 415-440.
46. B. H. Ji and H. J. Gao, *J. Mech. Phys. Solids*, 2004, **52**, 1963-1990.
47. R. Z. Wang, Z. Suo, A. G. Evans, N. Yao and I. A. Aksay, *J. Mater. Res.*, 2001, **16**, 2485-2493.

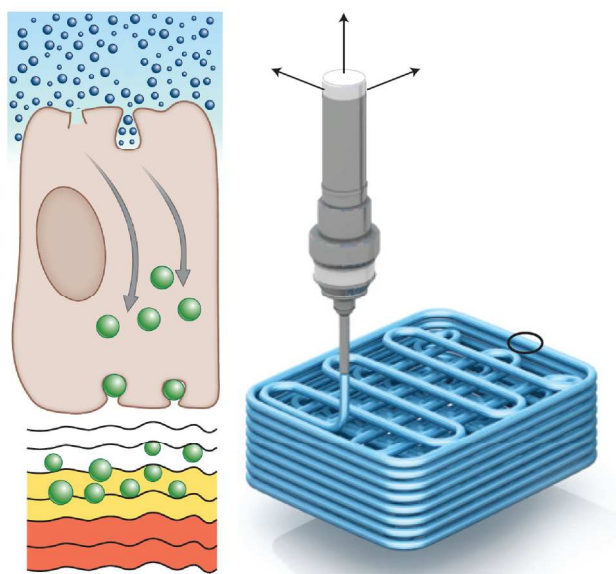
48. H. D. Espinosa, A. L. Juster, F. J. Latourte, O. Y. Loh, D. Gregoire and P. D. Zavattieri, *Nat. Commun.*, 2011, **2**.
49. F. Song and Y. L. Bai, *J. Mater. Res.*, 2003, **18**, 1741-1744.
50. E. L. Doubrovski, E. Y. Tsai, D. Dikovskiy, J. M. P. Geraedts, H. Herr and N. Oxman, *Comput. Aided Des.*, 2015, **60**, 3-13.
51. N. Oxman, *Virtual Phys. Prototyp.*, 2011, **6**, 3-31.
52. S.-P. Chen, H.-L. Chiu, P.-H. Wang and Y.-C. Liao, *ECS J. Solid State Sci. Technol.*, 2015, **4**, P3026-P3033.
53. P. Olla, *IEEE Technol. Soc. Mag.*, 2015, **34**, 74-80.
54. J. A. Lewis, *Adv. Funct. Mater.*, 2006, **16**, 2193-2204.
55. G. M. Gratson, M. J. Xu and J. A. Lewis, *Nature*, 2004, **428**, 386-386.
56. J. E. Smay and J. A. Lewis, in *Ceramics and Composites Processing Methods*, eds. N. P. Bansal and A. R. Boccaccini, John Wiley & Sons, Inc., 2012, DOI: 10.1002/9781118176665.ch13, pp. 459-484.
57. J. Cesarano, R. Segalman and P. Calvert, *Ceram. Ind.*, 1998, **148**, 94.
58. J. Cesarano, *MRS Online Proceedings Library Archive*, 1998, **542**, 133.
59. J. E. Smay, J. Cesarano and J. A. Lewis, *Langmuir*, 2002, **18**, 5429-5437.
60. E. B. Duoss, M. Twardowski and J. A. Lewis, *Adv. Mater.*, 2007, **19**, 3485-+.
61. G. Gratson and J. A. Lewis, *Langmuir*, 2005, **21**, 457-464.
62. J. C. Conrad, S. R. Ferreira, J. Yoshikawa, R. F. Shepherd, B. Y. Ahn and J. A. Lewis, *Curr. Opin. Colloid Interface Sci.*, 2011, **16**, 71-79.

63. B. Y. Ahn, E. B. Duoss, M. J. Motala, X. Guo, S. Park, Y. Xiong, J. Yoon, R. G. Nuzzo, J. A. Rogers and J. A. Lewis, *Science*, 2009, **323**, 1590-1593.
64. K. E. Easterling, R. Harrysson, L. J. Gibson and M. F. Ashby, *Proc. R. Soc. Lond. A Math. Phys. Sci.*, 1982, **383**, 31-41.
65. N. A. Fleck, V. S. Deshpande and M. F. Ashby, *Proc. R. Soc. Lond. A Math. Phys. Sci.*, 2010, **466**, 2495-2516.
66. K. V. Wong and A. Hernandez, *ISRN Mech. Eng.*, 2012, DOI: doi:10.5402/2012/208760, Article ID 208760.
67. N. Guo and M. C. Leu, *Front. Mech. Eng.*, 2013, **8**, 215-243.
68. J. R. Tumbleston, D. Shirvanyants, N. Ermoshkin, R. Januszewicz, A. R. Johnson, D. Kelly, K. Chen, R. Pinschmidt, J. P. Rolland, A. Ermoshkin, E. T. Samulski and J. M. DeSimone, *Science*, 2015, **347**, 1349-1352.
69. S. Kumar, M. Hofmann, B. Steinmann, E. J. Foster and C. Weder, *ACS Appl. Mater. Interfaces*, 2012, **4**, 5399-5407.
70. R. M. Erb, R. Libanori, N. Rothfuchs and A. R. Studart, *Science*, 2012, **335**, 199-204.
71. T. P. Niebel, F. J. Heiligtag, J. Kind, M. Zanini, A. Lauria, M. Niederberger and A. R. Studart, *RSC Adv.*, 2014, **4**, 62483-62491.
72. M. R. Sommer, R. M. Erb and A. R. Studart, *ACS Appl. Mater. Interfaces*, 2012, **4**, 5086-5091.
73. R. M. Erb, J. Segmehl, M. Schaffner and A. R. Studart, *Soft Matter*, 2013, **9**, 498-505.
74. R. M. Erb, J. Segmehl, M. Charilaou, J. F. Loffler and A. R. Studart, *Soft Matter*, 2012, **8**, 7604-7609.
75. M. Mirkhalaf, A. K. Dastjerdi and F. Barthelat, *Nat. Commun.*, 2014, **5**, Article number 3166.

76. A. R. Studart, *Angew. Chem. Int. Ed.*, 2015, **54**, 3400-3416.
77. B. N. Peele, T. J. Wallin, H. Zhao and R. F. Shepherd, *Bioinspir. Biomim.*, 2015, **10**, 055003.
78. B. Rackham, C. Piccolpasso, A. Van de Put, Victoria and A. Museum, *The Three Books of the Potter's Art, which Treat Not Only of the Practice But Also Briefly of All the Secrets of this Art*, Curwen Press, 1934.
79. J. S. Reed, *Introduction to the Principles of Ceramic Processing*, Wiley, 1988.
80. Y. N. Kryuchkov and T. L. Neklyudova, *Glass Ceram.*, 2015, **71**, 324-326.
81. I. A. Aksay and C. H. Schilling, eds., *Colloidal Filtration Route to Uniform Microstructures*, Wiley, New York, 1984.
82. D. S. Adcock and I. C. McDowall, *J. Am. Ceram. Soc.*, 1957, **40**, 355-362.
83. F. M. Tiller and C. D. Tsai, *J. Am. Ceram. Soc.*, 1986, **69**, 882-887.
84. W. Yang, I. H. Chen, B. Gludovatz, E. A. Zimmermann, R. O. Ritchie and M. A. Meyers, *Adv. Mater.*, 2013, **25**, 31-48.
85. I. Burgert and P. Fratzl, *Integr. Comp. Biol.*, 2009, **49**, 69-79.
86. D. Raabe, C. Sachs and P. Romano, *Acta Mater.*, 2005, **53**, 4281-4292.
87. J. C. Weaver, G. W. Milliron, A. Miserez, K. Evans-Lutterodt, S. Herrera, I. Gallana, W. J. Mershon, B. Swanson, P. Zavattieri, E. DiMasi and D. Kisailus, *Science*, 2012, **336**, 1275-1280.
88. L. A. Cheng, A. Thomas, J. L. Glancey and A. M. Karlsson, *Compos. Part A Appl. Sci. Manuf.*, 2011, **42**, 211-220.
89. L. K. Grunenfelder, N. Suksangpanya, C. Salinas, G. Milliron, N. Yaraghi, S. Herrera, K. Evans-Lutterodt, S. R. Nutt, P. Zavattieri and D. Kisailus, *Acta Biomater.*, 2014, **10**, 3997-4008.

90. S. Amini, A. Masic, L. Bertinetti, J. S. Teguh, J. S. Herrin, X. Zhu, H. B. Su and A. Miserez, *Nat. Commun.*, 2014, **5**.
91. S. Amini, M. Tadayon, S. Idapalapati and A. Miserez, *Nat. Mater.*, 2015, **14**, 943-+.
92. E. E. de Obaldia, C. Jeong, L. K. Grunenfelder, D. Kisailus and P. Zavattieri, *J. Mech. Behav. Biomed. Mater.*, 2015, **48**, 70-85.

Graphical and textual abstract for the contents pages



Analogous to the layer-by-layer and site-specific deposition of building blocks carried by living organisms during biomineralization (left), additive manufacturing technologies offer a compelling route for the fabrication of bioinspired heterogeneous architectures for next generation composite materials (right)